[1]Prof. Aishwarya Katkar[1*]

Prof. Dr. Sudha Rathod[2]

Dr. Ashish Jain[3]

Prof. Puja Vyawhare[4]

Ms. Anjali Rai[5]

Swathi J. Uttarwar[6]

QBD-Based Approach for Formulation Development of Docetaxel-Loaded Solid Lipid Nanoparticles in Combination with Herbal Extracts for Breast Cancer

Abstract: - In line with a Quality by Design approach, this study developed docetaxel-encapsulated solid lipid nanoparticles (SLNs) with herbal extracts for improved breast cancer treatment safety and efficacy. The solvent emulsification and ultrasonication-prepared SLNs are used for increasing the solubility of docetaxel, overcoming chemoresistance, and minimizing toxicity. Proper study of preparation factors helped in achieving better control over the size of the nanoparticles, percentage of encapsulation, as well as release. The optimized nanocarriers possessed stability, high loading of docetaxel, sustained release, and enhanced anticancer effects when conjugated with antitumor herbs. In summary, this work establishes the co-delivery of breast cancer treatment through encapsulating chemotherapeutic drugs with natural compounds using targeted SLNs. Nanoformulation has a positive impact on pharmacotherapy as it leads to an increase in the bioavailability and specificity of tumor tissue and reduces general toxicity. More possibilities can be seen in other chemorefractory cancers and better patient concordance along with therapeutic efficacy achieved through combinational drug delivery. More large-scale production and preclinical studies could pave the way for the clinical application of this integrated strategy using QbD Design nanoparticles in the fight against lethal carcinoma.

Keywords: SLN, docetaxel, herbal extracts, breast cancer, chemoresistance, QbD

Introduction

Breast cancer is among the common cancers that affect women globally contributing to about 25% of all cancer incidences and 15% of all cancer mortalities as indicated in global statistics (Siegel et al., 2020). These conventional treatments include surgery, radiation, chemotherapy, hormone therapy, and targeted therapy. Nonetheless, most of these approaches are nonselective for tumor tissues and are accompanied by numerous side effects that greatly reduce patients' quality of life (Tang et al., 2017). Despite the progress, breast cancer is still a significant health issue indicating the necessity for using safer and efficient treatments, particularly in the later levels of breast cancer metastasis (Cardoso et al., 2020).

Some examples of nanotechnology-based drug delivery systems include solid lipid nanoparticles (SLNs), which have proven effective in treating breast cancer. SLNs are generally made up of a solid lipid phase, which is stabilized by surfactants and possesses some characteristics that make them suitable for the delivery of anticancer drugs such as Small size for passive targeting using the EPR effect, ease in large-scale production, increased solubility of drugs, sustained release, increased stability of the drug and ability to control the kinetics of the release of the drug (Müller et al., 2000 Additionally, combination therapies with multiple drugs or use of a new adjuvant is becoming a focus of much attention as ways of enhancing the effectiveness of the drug while at the same reducing the side effects (Anayyat et al., 2023). Different groups of herbal extracts have also shown anticancer effects against breast cancer and other types of cancer by increasing cancer cell cytotoxicity, inhibiting proliferation, and altering the molecular pathways related to carcinogenesis and angiogenesis, etc However, the major issue that restricts their therapeutic potential is their poor solubility (Han et al., 2011).

[1*]Assistant Professor, Shri D D Vispute College of Pharmacy & Research Center, New Panvel,mail id: aishwaryamane1992@gmail.com

[2]Principal, OES Oriental College of Pharmacy, Navi Mumbai, mail id: sudharathod@gmail.com

[3]Principal, Shri D D Vispute College of Pharmacy & Research Center, New Panvel,mail id: ashish_aeish@rediffmail.com

[4]Yadavrao Tasgaonkar Institute Of Pharmacy, Karjat, Mail id: vyawharepooja@gmail.com

[5]Assistant Professor, OES Oriental College of Pharmacy, Navi Mumbai, mail id: anjali.rai@ocp.edu.in

[6]Asst Professor, Shri D D Vipsute College of Pharmacy, New Panvel, Mail Id: swathikommawar@gmail.com

Hence, the conjugation of anticancer drugs and herbal extracts into SLNs may help to eradicate the limitations accompanying free drugs and each therapy. Docetaxel belongs to the group of chemotherapeutic agents applied for breast cancer treatment with high frequency. It interferes with microtubule organization, which in turn halts cell division and induces cell death. However, its clinical application is restricted due to its insolubility in aqueous media, high toxicity if administered systemically, and chemoresistance (Koopai et al., 2011). The use of docetaxel-loaded SLNs may improve its therapeutic efficacy against chemotherapy-resistant breast cancer subtypes without causing toxicity to normal tissues (Naguib et al., 2014). Adding docetaxel to SLNs formulated with herbal extracts that exert synergistic anticancer effects may enhance the therapeutic efficacy of SLNs against breast cancer.

Quality by design (QbD) is a risk-based approach that has been recommended by regulatory agencies for the development of pharmaceutical processes. It involves determining formulation and process criticality and understanding how they affect key characteristics of the final product. The significant goal is to identify the design space and control approach that will lead to high product quality (Soni et al., 2020). QbD principles can therefore be applicable in the development of SLN formulations to result in a more consistent product performance.

Some of the nanoparticle systems that have been discussed in QbD-based studies include polymeric nanoparticles, nanocrystals, nanoemulsions, and lipid–polymer hybrid nanoparticles (Kumari et al., 2011). Despite the potential of such formulations in breast cancer therapy, there is a lack of reports on QbD approaches for docetaxel-loaded SLNs combined with herbal extracts.

The main objective of this work is to design and characterize a solid lipid nanoparticle system containing docetaxel and selected herbal extracts for breast cancer treatment based on a QbD approach. Specific aims are: The specific objectives are: (1) To select possible herbal extracts for breast cancer treatment based on in vitro antiproliferative activity against breast cancer cell lines; (2) To formulate docetaxel incorporated SLNs using solvent emulsification technique followed by ultrasonication with the selected herbal extracts; (3) To systematically investigate effects of formulation and process factors on functional properties and drug release profile using QbD approach (4).

Materials: Drug, Excipients, Herbal Extracts

Experimental: Preparation of optimization batches

Herbal Extracts: Withania Somnifera & Papain

The formulation batches of F1 to F12 had different compositions in terms of the total lipid and liquid lipid percentages and were 66.67% to 84.62% and 50% to 58.33%, respectively. The EE was observed to improve with the increase in the percentage of total lipid, from 56 % for F1 up to 87% for batches F10-F12. On the other hand, the mean particle size (MPS) reduced from 293 nm to 113 nm in Table 1. Therefore, higher total lipid and higher EE were obtained although the particle size was smaller at the highest lipid percentages.

Table 1. Formulation Batches data for QbD

BATCHES	% of Total Lipid	% of Liquid Lipid	% EE	MPS
F1	66.67	50	56	293
F2	66.67	62.5	60	285
F3	71.43	50	65	299
F4	75.00	50	79	261
F5	75.00	58.33	82	255
F6	77.78	50	85	230
F7	80.00	50	89	177
F8	80.00	56.25	88	170
F9	81.82	50	87	165
F10	83.33	50	87	123
F11	83.33	55	86	125
F12	84.62	50	86	113

Formulation Of Docetaxel Loaded SLN Containing Withania Somnifera & Papain

Figure 1, describes the procedure of preparing the SLNs in terms of several steps. First, the required amounts of the drug and lipids were weighed based on the desired drug-to-lipid ratio. The drug and lipids were then dissolved in 20ml of ethanol and the mixture was sonicated until the drug and lipids were fully dissolved. Then 80 ml of phosphate buffer saline (PBS) with pH 7.4 and 3 ml of Tween 80 were added to the mixture and sonicated again till an emulsion was formed. The obtained emulsion solution was then subjected to bead milling for 2 hours to achieve better particle size reduction and uniformity. After 2 hours of bead milling, Withania somnifera and the enzyme, papain were incorporated into the solution. Also, 5% mannitol was included as the cryoprotectant in the culture medium. After that, the final solution was transferred to a deep freezer where it was kept at -18°C for 24 hours to freeze. After 24 h, the frozen solution was further lyophilized in a freeze dryer for another 24 h under a vacuum of 1 kPa to get a dry powdery form of the formulation. This final dry powder formulation was then stored in a deep freezer for later purposes as well as for further testing. The above-mentioned process allowed to preparation of solid lipid nanoparticles that may improve the stability, bioavailability, and therapeutic effectiveness of drugs. Using ethanol dissolution, sonication, bead milling, freezing, and lyophilization processes, the key steps helped to create uniform nanoparticles with the desired properties.

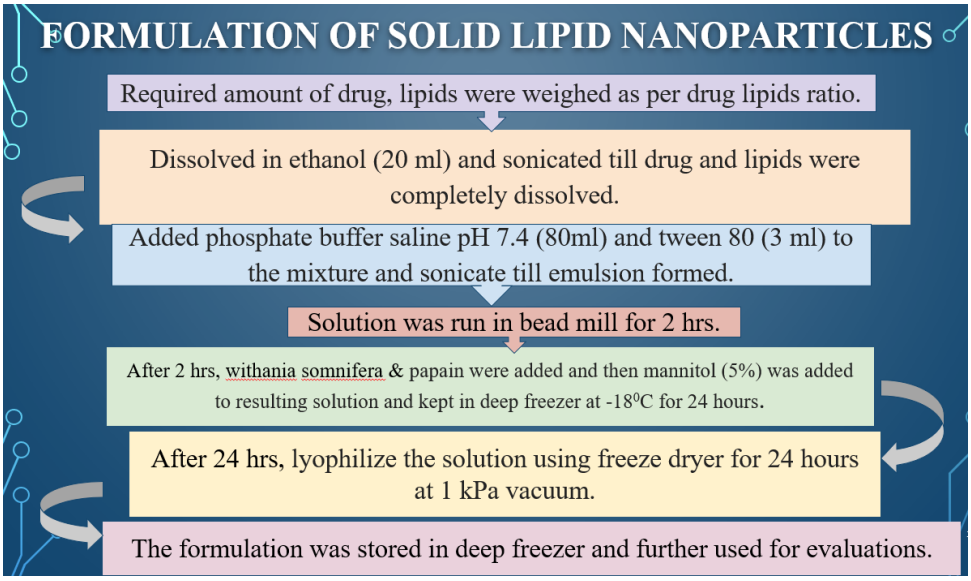

Figure 1. Formulation of Solid-Lipid Nanoparticle

Factorial Experimental Design in the Optimization of Nanoparticle Formulation

Optimization was done using a 2 x 2 factorial design. The influence of independent process parameters of the Drug. Thus, the study was done to determine the effect of; Lipid ratio (X1) and solid lipid: liquid lipid ratio (X2) on the dependent parameters of; Particle size (Y1) and entrapment efficiency (Y2) at three levels. The concentration of the drug and the temperature at which the processing was done were controlled. To obtain the best-fitting model, the polynomial equation, perturbation plots, interaction plots, 3D response curves, and overlay plots for a given statistical model, the Design-Expert software (Version 13; Stat-Ease Inc, USA) was utilized. In determining the optimum levels of the set factors, the p-value was set at <0.05. The particle size and entrapment efficiency were determined at different levels of the factors: A, B, and AxB. The study sought to establish the right formulation conditions that would lead to small particle sizes with high entrapment efficiency. The analysis of the software allowed the establishment of the best combination of factor levels for the response variables. The use of factorial design made it possible to determine the effects of different independent variables systematically.

The parameters included two independent variables—drug to lipid ratio (X1) and solid lipid to liquid lipid ratio (X2)—with three coded levels for each: Essentially, it is a -1 for low, 0 for medium, and +1 for high. In this study, the two dependent variables that were used to assess the nanoparticles were, particle size in nanometers (Y1) and drug entrapment efficiency in percentage (Y2). The independent variables and their coded levels were chosen to measure the impact that changing the ratio of the major components of the nanoparticle formulation would have.

The low, medium, and high settings allowed systematic changes in the ratios to investigate whether nanoparticle size and drug loading are impacted in Figure 2. Experimental design matrices are typically utilized in formulation development investigations to test a range of formulations without having to alter components singly while enduring several tests. The amount of measurement of Y1 and Y2 resulting from measurements of the different combinations of X1 and X2 levels could be subjected to statistical analysis to arrive at the best formulation of the nanoparticles. This approach allowed the subsequent evaluation of the effects of drug content and lipid composition on the primary attributes of nanoparticles.

Independent Parameter	Levels (Coded)		
	low	Medium	High
X1: Drug : Lipid	-1	0	1
X2: Solid Lipid : Liquid Lipid	-1	0	1
Dependent Parameter			
Y1: Particle Size nm			
Y2: Entrapment Efficiency %			

Figure 2. Experimental design matrix for a study of lipid nanoparticles for drug delivery

An experimental design was employed to investigate the impact of two factors, namely factor A and factor B on the characteristics of solid lipid nanoparticles. In particular, the researchers investigated how different levels of factors A and B affect the entrapment efficiency (EE%) and the mean particle size (MPS) of the developed nanoparticles. A three-factor factorial design was used and nine experimental runs were performed with each factor being at low (-1), medium (0), and high (1) coded levels. The results were summarized in a tabular format that depicted the factor combinations for the run and the corresponding EE% and MPS values in nanometers. When factor A was low (-1) and B was medium (0) in run 3, the nanoparticles had an EE% of 60% and MPS of 285 nm. The table showed that as factor A progresses from low to high, the EE% is consistently raised at the expense of the MPS. For instance, in run 5, while A was at its maximum level of 1, B was at the lowest level of -1, the highest EE of 89%, and the smallest MPS of 177 nm was obtained in Figure 3. In general, the central run 4 with both factors at 0 levels provided the intermediate EE% of 82% and MPS of 255 nm. The findings indicated that factor A affected both responses to a greater extent than factor B within the experimental domain. However, to establish the factor effects and interactions conclusively, more statistical analysis would be required. This factorial experiment showed the possibility of different formulation or process factors on the quality attributes of the solid lipid nanoparticles.

Run	Factor 1 A:A	Factor 2 B:B	Response 1 EE %	Response 2 MPS nm
1	0	-1	79	261
2	0	1	85	230
3	-1	0	60	285
4	0	0	82	255
5	1	-1	89	177
6	-1	1	65	299
7	1	1	87	165
8	1	0	88	170
9	-1	-1	56	293

Figure 3. Model – Design Space

Characterization of docetaxel loaded SLN: % EE, Drug loading

The EE and drug loading of the docetaxel-loaded SLN formulations were also quantified. The formed SLN dispersions were subjected to centrifugation at 20,000 rpm for 90 minutes at 10°C to pellet down the encapsulated docetaxel from the free drug. The concentration of free docetaxel in the supernatant was subsequently determined by high-performance liquid chromatography (HPLC). EE was calculated using the equation: EE% = Total drug – Free drug/Total drug x 100. To assess the drug loading, the content of docetaxel in the lyophilized SLN was analyzed by HPLC after dissolving the sample with acetonitrile. Drug entrapment efficiency was determined as the amount of docetaxel encapsulated per hundred milligrams of lipid. Analysis of variance was done using the one-way ANOVA test while all measurements were done in triplicate and results were presented as mean ± standard deviation. The data obtained was further subjected to analysis of variance through Design Expert software to determine the significance of the formulation parameters on EE and drug loading.

Statistical analysis of data using DOE Software

The experimental results of entrapment efficiency (EE%) and mean particle size (MPS) from nine different formulation runs were analyzed statistically using Design Expert software version 13 (Stat-Ease Inc, USA). A 3-factor 2-level full factorial design was used to study the main effects of X1 and X2 and their interaction effects on the EE% and MPS of the formulations. The data collected was then fitted into different models and a backward regression analysis was used to obtain the best-fitting equation. There was significant variability in the nanoparticle properties due to the study factors and their interactions, which was determined by performing the analysis of variance (ANOVA). To get a better perception of the effect of the formulation parameters on the responses, three-dimensional response surface plots were generated using the software. The target was to achieve as low an MPS as possible while attaining the highest possible EE%. Finally, numerical optimization was performed to arrive at the optimum levels of X1 and X2 to obtain the required nanoparticle attributes.

Result & Discussion

% EE: Percentage Encapsulation Efficiency

Response results – Entrapment efficiency

The quadratic model on the response variable “EE” has a table of ANOVA, which consisted of the sources of variation, which included linear terms for factors A and B, interaction between A and B, quadratic terms A and B, residual variation not covered by the model, total variation, sums of squares indicating variation from each source, the degrees of freedom, mean squares that estimated variance, F-statistic, and the probability of randomness or p.

The results of the regression analysis revealed that the coefficients for the linear terms of A and B, their interaction term, and the quadratic term of A were significant at $p < 0.05$ level. However, the quadratic term for B was not significant, the p-values were 0.8008. The overall significance of the model was also very high as indicated by the F-test with the model F-value at 363.47 and a p-value of 0.0002.

The explanation provided in the additional materials stressed the increased importance of the general model and the specified terms with a p-value of less than 0.05. It stated that it is possible to prune non-significant terms such as B-squared to enhance the performance of the model. The ANOVA table and the write-up of this work showed that this quadratic model and the major terms that made it up were very efficient in accounting for the variation that was identified in the response variable EE.

ANOVA for Quadratic model

Response 1: EE

	Source	Sum of Squares	df	Mean Square	F-value	p-value	
	Model	1329.36	5	265.87	363.47	0.0002	significant
	A-A	1148.17	1	1148.17	1569.65	< 0.0001	
	B-B	28.17	1	28.17	38.51	0.0084	
	AB	30.25	1	30.25	41.35	0.0076	
	A^2	122.72	1	122.72	167.77	0.0010	
	B^2	0.0556	1	0.0556	0.0759	0.8008	
	Residual	2.19	3	0.7315			
	Cor Total	1331.56	8				

Factor coding is **Coded**.
Sum of squares is **Type III - Partial**

The **Model F-value** of 363.47 implies the model is significant. There is only a 0.02% chance that an F-value this large could occur due to noise.

P-values less than 0.0500 indicate model terms are significant. In this case A, B, AB, A^2 are significant model terms. Values greater than 0.1000 indicate the model terms are not significant. If there are many insignificant model terms (not counting those required to support hierarchy), model reduction may improve your model.

Figure 4. ANOVA for Quadratic model

The model fit statistics that estimated the goodness of fit and prediction of a regression model. The standard deviation of 0.8553 meant that on average, the actual data points were less than one unit off from the model's predicted values, which was favorable. The mean response was 76.78 which was used to give a central value for the data collected. The value of CoV was equal to 1.11%, which indicated that the standard deviation was 1% more than the mean, and this demonstrated that the models were performing similarly close to the average in Figure 5.

The R-squared of 0.9984 indicated that 99.84% of the variation in the response variable could be attributed to the predictors. This extremely high value indicated that we had a very good fit for the model. The value of the adjusted R-squared of 0.9956 was adjusted for the number of variables, thus it remained very high but not overly, to avoid overfitting. The predicted R-squared value was 0.9800 indicating rather high predictive power on new data but slightly lower than the adjusted R-squared as expected. Lastly, the adequate precision was 47.4948, which was greatly higher than the acceptable level of 4, meaning that the test had a good signal-to-noise ratio and a high ability to predict results.

It mentioned that the value of the delta between the predicted and adjusted R-squared was below 0.2, meaning good generalization without much overfitting. To sum up, fit statistics used in the past tense revealed that the chosen models provided high accuracy, predictiveness, low error rates, and close to one R-squared metric accompanied by a high value of the precision ratio.

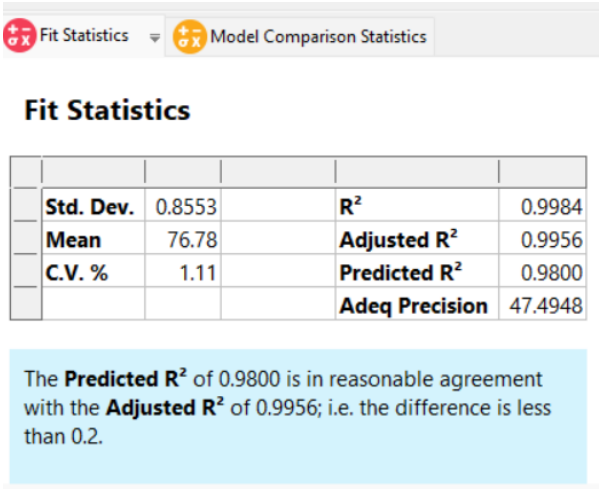

Figure 5. Fit statistics

The final equation of factors for a quadratic model that has anticipated the response variable EE which could be energy efficiency or any other depending on the context. The equation predicted the interaction between EE and two independent variables A and B by embedding linear terms, interaction terms, and squared terms in the quadratic form.

The Equation:

$$EE = 81.88889 + 13.83333 \cdot A + 2.16667 \cdot B - 2.75000 \cdot (A \cdot B) - 7.83333 \cdot A^2 + 0.16$$

The intercept was 81.88889, which is the starting estimate of EE when both A and B are zero. The coefficient of factor A was 13.83333 × A, which means for every unit change in A, EE changes by 13.83 units if the other variables were held constant. This was a direct linear effect of factor B equal to 2.16667 × B, which means that for every unit increase in B, EE would increase by 2.17 units of measure. The interaction term between A and B was calculated as (-2.75000) * (A × B). The result of the interaction term was negative (-2.75) suggesting that while both factors were positive, their net effect was slightly negative on EE in Figure 6.

The quadratic effect of A was -7.8333300000000 × A2. The negative sign suggested that the impact of A had a negative correlation with EE, which is consistent with a quadratic function. The quadratic term of B was equal to 0.166667 multiplied by B2. Its positive sign indicated that as B rose, EE also rose slightly at an increasing rate, albeit to a very small extent. Since the coefficients for A, and B and their interaction were all significant, it meant that these factors were relevant for having predicted EE.

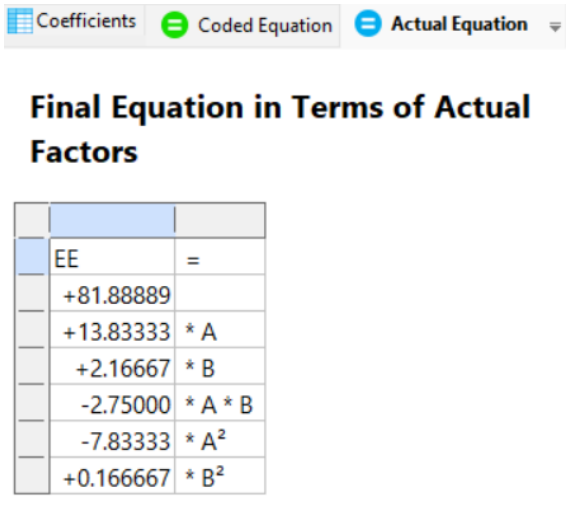

Figure 6. Actual factors equations for EE

Model graphs - Entrapment efficiency

The figure displayed a Perturbation Plot of two variables, A and B which influenced the response of encapsulation efficiency (EE) percentage. The EE percentage shown on the y-axis indicated the efficiency of encapsulation in percentage level from 50% to 90%. The x-axis expressed the difference of factors A and B from the center on the coded units scale of -1 to 1. There were two curves - a green curve for Factor A and a blue curve for Factor B A green curve was drawn starting from a lower efficiency value of around 60% for deviation -1 and rising steeply to around 80% for deviation 0. It then tapered off a bit but rose again and became slightly positive as the deviation was taken. However, the curve of the blue color stayed at a figure of approximately 80% throughout the range suggesting that Factor B did not notably affect the response at the range in question. In the plot of the story, the black dot at 0 deviations for both factors A and B stood for the average or base value of the response. It was also evidence that Factor A (green curve) had a higher non-linear relationship on the encapsulation efficiency percentage than Factor B (blue curve) which had a minimal impact.

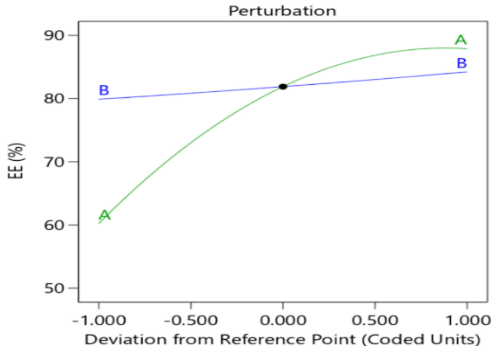

Figure 7. Perturbation Plot with two factors (A and B) affecting the response variable **EE (%)**, which appears to represent "encapsulation efficiency" or a similar efficiency measure

Figure 8, depicts a contour plot that represents the overall impact of the two factors: A and B on the response factor: encapsulation efficiency (EE) percentage. The horizontal axis displayed Factor A on coded units of -1 to 1 while the vertical axis displayed Factor B on the same coded units. The color gradient varied by the EE percentage: blue for 50%, green for 70%, and red for 90%. Other contour lines were drawn on values like 60%, 70% and 80% which represented the EE levels as the factors were varied. Red dots indicated the actual measured design points from experiments placed at discrete locations within the plot boundary.

As for Factor A, it seemed to have a greater impact on enhancing EE because efficiency jumped significantly when A shifted from -1 to 1. The change in B seemed to have a lesser effect on the overall Values of EE with fewer fluctuations observed. The contour plot depicted how the two factors A and B influenced the encapsulation efficiency; the area shaded in red at the upper right corner represented the highest EE values. This contour plot depicted how these two factors affected the encapsulation efficiency percentage using an experimental design. The measurements and visualizations helped to identify the necessary factor settings for further enhancement of the response.

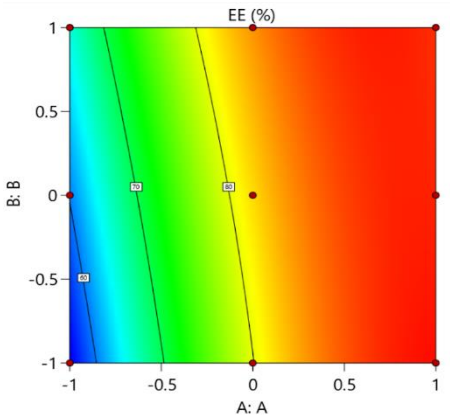

Figure 8. Contour plot

MPS: Mean Particle Size

Figure 9 was a Predicted vs Actual Plot which compares the real values of the experiment to the values predicted by the model. The x-axis was the actual experimental values, which were scaled between 50 and 90. The y-axis reflected the predicted values derived from the model, which ranged from 50 to 90. A diagonal reference line was depicted where the predicted values would align with the actual values. If the points were closer to this line, it would mean that the model had good predictive accuracy. For situations at different levels, the data points are marked in red to blue according to the actual/predicted values. The red and orange points were found towards the lower end of the scale, between 50% and 60%. The green and yellow points were clustered to the middle range at approximately 70-80%. The blue points referred to the observed values which were slightly above 90%. The interpretation was that the data points were very close to the diagonal line, implying that the model predictions were very accurate and close to real values. The scoring of points close to the reference line suggested a small amount of difference between the forecasted and actual values. Such a plot was often applied in situations like regression analysis or model checking to ensure that the model was efficient.

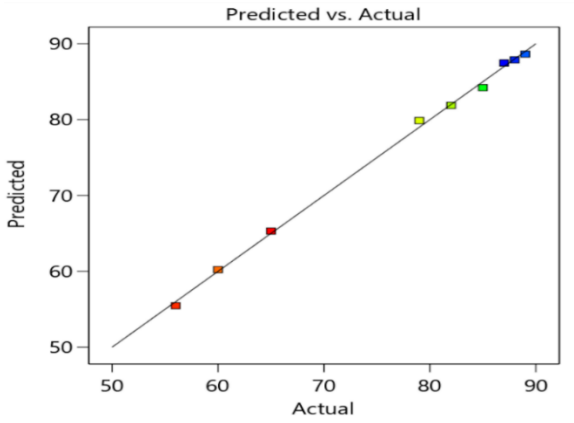

Figure 9. Predicted vs Actual Plot compares the experiment's real values to the predicted values by the model.

Figure 10 provided, which was a response surface of an efficiency variable (EE) on the third (z) axis with two independent variables on the first (x) and second (y) axes labeled A and B respectively. The first and second axes ranged from -1 to 1 while the third axis plot depicted the response from 60% to 100%. As can be observed in Figure 7, the surface represented the smooth transition of the EE along the z-axis from the lower-end blue area at about 60% EE to the higher-end red area at nearly 100%. There were different red data point markers in the plot to highlight where experiments or measurements could have been carried out. The gridlines curved upwards from lower to higher EE percentages and this indicated that the response variable increased with the independent variables. The base was gray-toned and the contour lines represented EE levels on the surface at various coordinates. In summary, the visualization illustrated how the efficiency was influenced by the two factors in the multivariate system that were represented by the response surface.

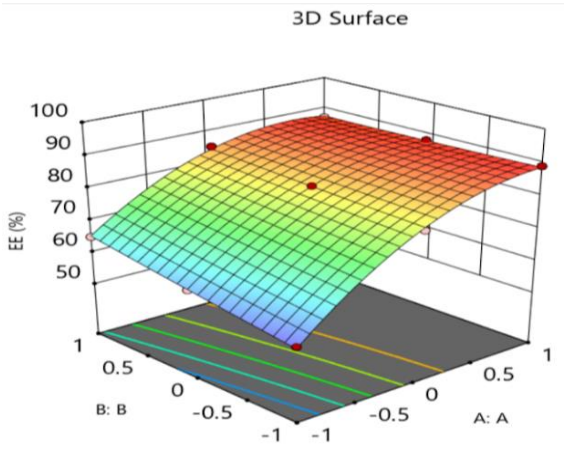

Figure 10. A three-dimensional surface (3D Surface)

Response results – Mean Particle Size

In the Analysis of Variance (ANOVA) table, a Quadratic model was checked with the response variable MPS. The model comprised the main effects of factors A and B (A, B), their interaction (AB), and the quadratic effects of each factor (A2, B2). The table showed the SS, df, MS, F-value, p-value and significance for each term and the residual, total and overall models.

For the linear regression of the full quadratic model, the overall model F-value was 34.53 with a significant p-value of 0.0075 and therefore, the full quadratic model was statistically significant in explaining the variation in MPS. Factor A had an F-value of 165.93 and a corresponding p-value of 0.0010, which pointed out its significance in the overall results. Nonetheless, factor B was statistically insignificant (p= 0.2827), the interaction between the factors AB (p= 0.4933) and the quadratic terms A2 (p= 0.1267) as well as B2 (p= 0.9253). The residual sum of squares was 401.44 with 133.81 mean square. The total variance accounted for by the model was 23505.56.

Assuming noise, the large F-value of 34.53 and low p-values suggested that the non-significant terms could be eliminated for model reduction. Finally, the ANOVA analysis showed that the linear factor A played a significant role in the variation of the response, MPS. The interpretation offered insight into what should be done in the next phase of enhancing and refining the quadratic model.

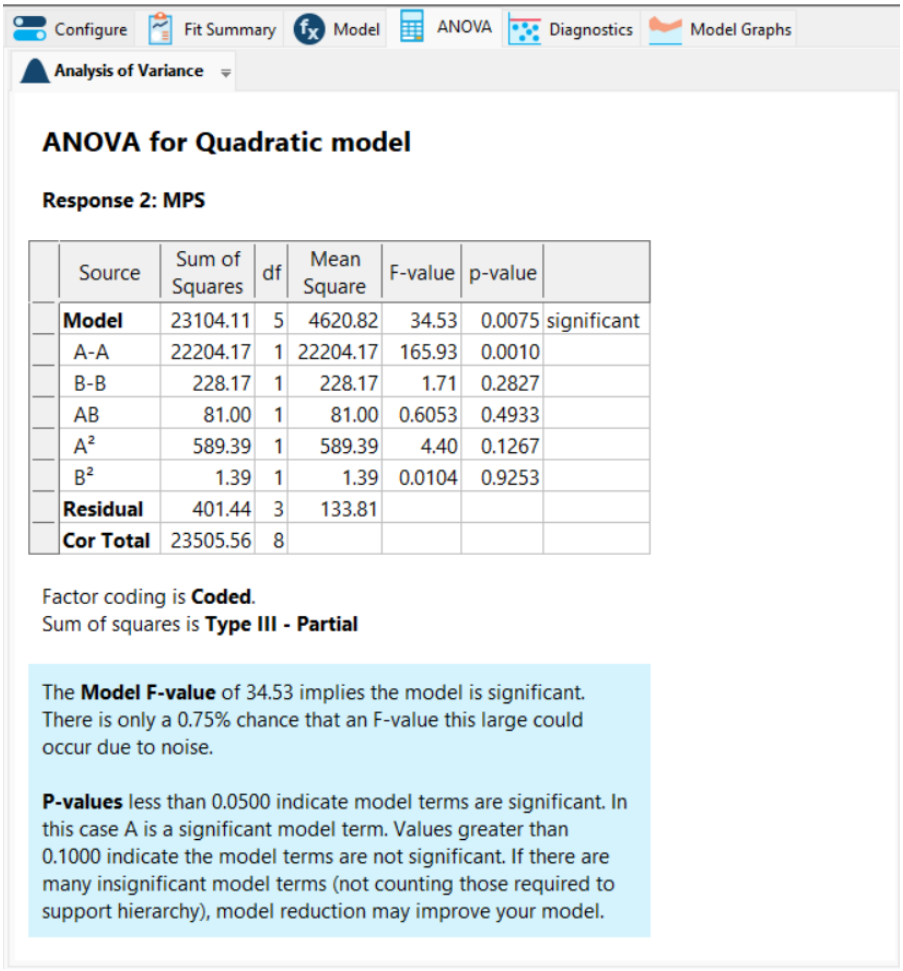

Figure 11. Analysis of the Quadratic model

The Fit Statistics of the model which seems to be an econometric model, probably a regression model based on the data presented earlier. The table included the important statistical parameters used for measuring the fitness of the model. The mean value of the residuals, signifying the difference between actual and predicted values, was 11.57 for the standard deviation. This lower value indicated that the actual values were closer to the model's output as compared to the previous case. The mean of the observed data was 237.22, which provided a point of reference of the scale of the data. It was established that the coefficient of variation, which is the standard deviation divided

by the mean and expressed in percentage, was 4.88. This lower C.V. indicated that the model was a better representation of the data concerning the variability. The R-squared was 0.9829. This stands for the extent to which the variation observed in the dependent variable (response) was explainable by the independent variables. From the data, an R2 value of 0.9829 showed that 98.29% of the variation in the response variable was explained by the model which was very satisfactory. The adjusted R2 of 0.9545 indicated that despite the number of terms included in the model, the fit remained excellent. The cross-validated R2 of 0.8134 showed how well the model performs for new data or how good the model is in terms of overfitting the data used in model fitting. This was further supported by the high predicted R2 of 0.8134, which portrayed a good predictive nature. The Adequate Precision was 14.1873 and it calculated the signal-to-noise ratio of the data set. A ratio above 4 was preferred, which was a measure of the model's accuracy. A perfect value of 14.1873 indicated a high level of reliability of the proposed model.

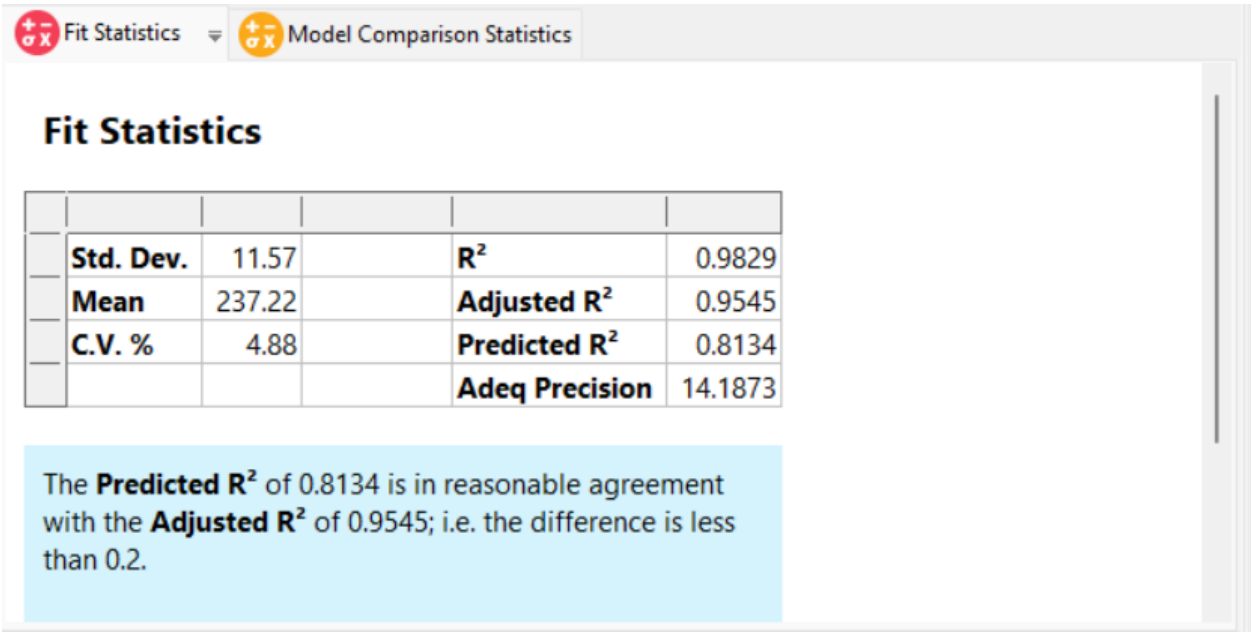

Figure 12. Fit statistics analysis

Figure 13 provided by the presented table was named "Coefficients in Terms of Coded Factors." The content of the table aimed at presenting information about the coefficients of the dependent variable vs the coded factors A, B, AB, A2, B2, and their interaction. The columns of the table included the Factor, the Coefficient Estimate, the degrees of freedom (df), the Standard Error, the 95% Confidence Interval (Lower and Upper values), and the Variance Inflation Factor (VIF).

The intercept was estimated as 248.11 with a standard error of 8.62; the 95% confidence interval was between 220.67 and 275.55. Concerning the results of estimation for Factor A, the coefficient was -60.83 with a Standard error of 4.72 and 95% confidence interval of -75.86 and -45.80. For Factor B, the coefficient estimate was -6.17, the standard error was 4.72, and the 95% CI range was -21.20 to 8.86. The coefficient for the AB interaction term was -4.50, the standard error was 5.78, and the confidence interval was CI -22.91 to 13.91. Thus, the estimates for A2 and B2 were -17.17 and 0.8333 respectively, with the standard errors of 8.18 and using confidence intervals within about 25 of the coefficient values. It was also observed that all of the VIF values were 1.000; hence, revealing that there was no multicollinearity in the terms.

It revealed the statistical significance of coded factors and the dependent variable. The SEs, CIs, and VIF that were presented gave measures of the accuracy, imprecision, and orthogonality of the coefficients.

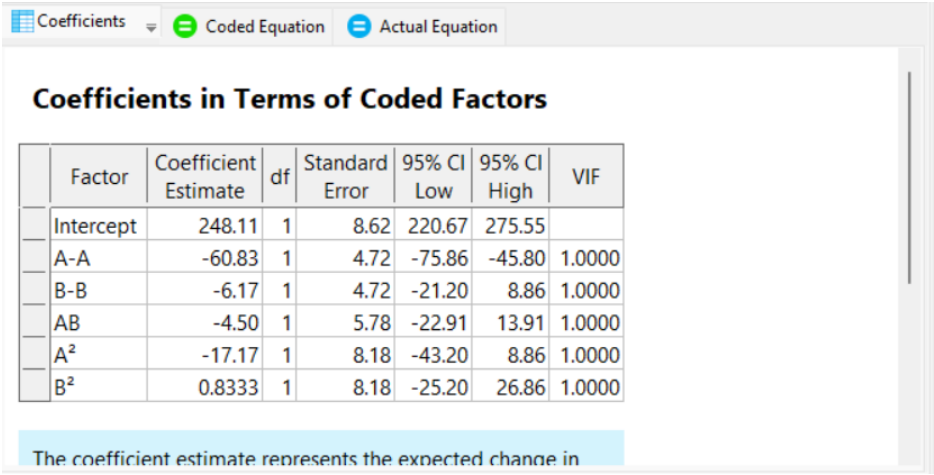

Figure 13. Coefficients in Terms

Figure 14 shows the Fit Statistics of a statistical model; most probably, a regression model based on the data shown earlier. The table included the measures that were used to evaluate the goodness of fit of the model. The residual standard error was 11.57, which meant that the actual values were close to the predicted ones in the model. Thus, the mean of the observed data was 237.22, which allowed us to use it as a reference point for understanding the scale of the data. The coefficient of variation, which is obtained by dividing the standard deviation by the means and then multiplying it by 100, was 4.88%. The lower C.V. indicated a better fit of the model given the variability of the data. The R-squared was 0.9829, therefore 98.29% of the changes in the response variable were explainable by the model, which implies a very strong fit. The value of the adjusted R-squared of 0.9545 made it clear that even when controlling for the number of predictors, the fit was still excellent. The cross-validation's predicted R-squared of 0.8134 evaluated the model's ability to generalize to new data to show that the model had good predictive power. The AP statistic of 14.1873 was the signal-to-noise ratio that showed that any figure greater than 4 was acceptable, and a high figure here confirmed the reliability of the model. Moreover, the value of Predicted R-squared and Adjusted R-squared was nearly close to each other and was not very high indicating that the model has not overfitted and possesses good variability for prediction. Therefore, the obtained high R-squared statistics, low coefficient of variation, good signal-to-noise ratio and a good agreement in the obtained predictive metrics suggested about an excellent overall fit and predictive model based on the data.

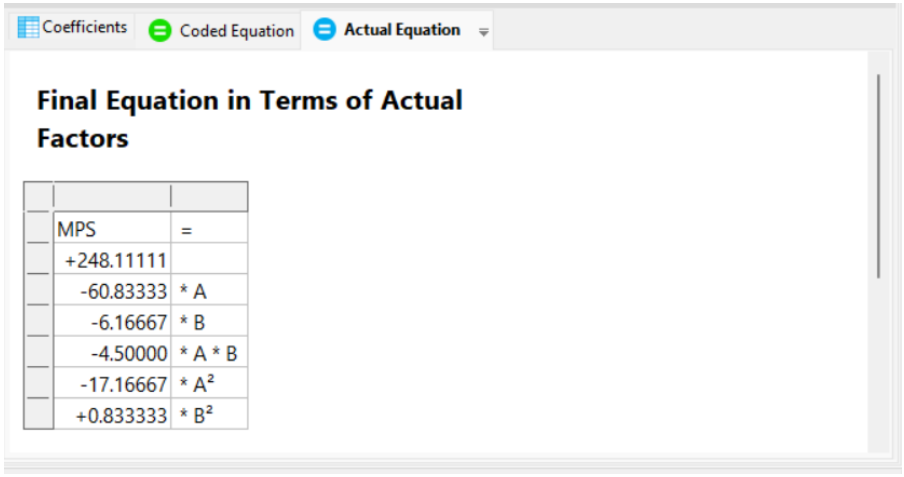

Figure 14. Equation actual factors

Model graphs- Mean Particle Size

Figure 15 identified a Perturbation Plot that reflected the impact of two factors A and B on the response variable MPS (nm); it was measured on the y-axis. The x-axis represented the Deviation from Reference Point in Coded Units which varied from -1.000 to 1.000. The plot was intended to show how the manipulation of factors A and B, concerning the point 0.000, affected the MPS in the past.

As expected, factor A had a negative and non-linear relationship with MPS, and it had a steep drop after a certain point. As the value of factor A went up from -1.000 to 1.000, the MPS went down which means that in the past much bigger values of A reduced MPS. This means that the line for factor B was almost horizontal, and this shows that it had a very weak or non-existent relationship with MPS over the same range of deviation. MPS did not fluctuate much, as factor B varied from a low of -1.000 to 1.000.

The black point at 0.000 corresponded to the coded value of zero for both factors, which illustrated the baseline MPS value of approximately 240 nm. Therefore, according to the observed Perturbation Plot, factor A had a strong effect on MPS in the past, and factor B had almost no effect within the range of deviation from the reference point.

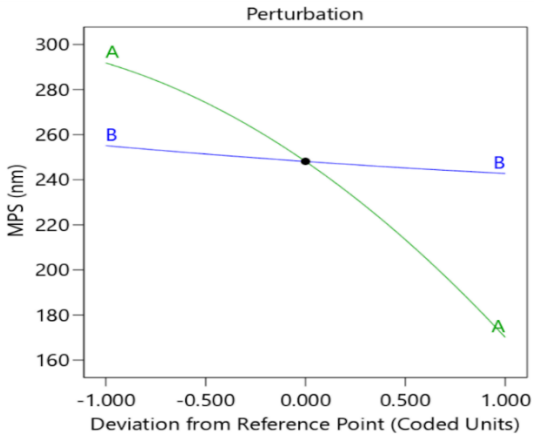

Figure 15. Perturbation Plot Showing the Effect of Variables A and B on Mean Particle Size (MPS)

It mapped two factors A and B and the response variable, MPS (nm), which was represented by colors on a contour plot. Factor A was represented on the x-axis, with values ranging from -1 to 1. Factor B was depicted on the y-axis, and it ranged between negative 1 and 1 as well. The contour lines depicted the different levels of the response variable MPS. It was changed from red color, which represents a higher value and approximately 299 nm for the maximum MPS to blue color, which represents a lower value and approximately 165 nm for the minimum MPS. The contour lines depicted values of the response variable as 280, 260, 240 nm, etc in Figure 16. Design points were specified by red dots distributed across the plot, which likely represented experimental or simulation data points for which the model was calibrated. The right panel with the label 'Factors Tool' allowed for modifying the values of factors A and B, marked as X1 and X2, and to move through distinct runs or contours of the plot. The contour plot showed the interaction of factors A and B while illustrating how MPS, the response variable, was affected. The fact that the contour line was linear meant that there was a strong relationship between these input factors and the output response.

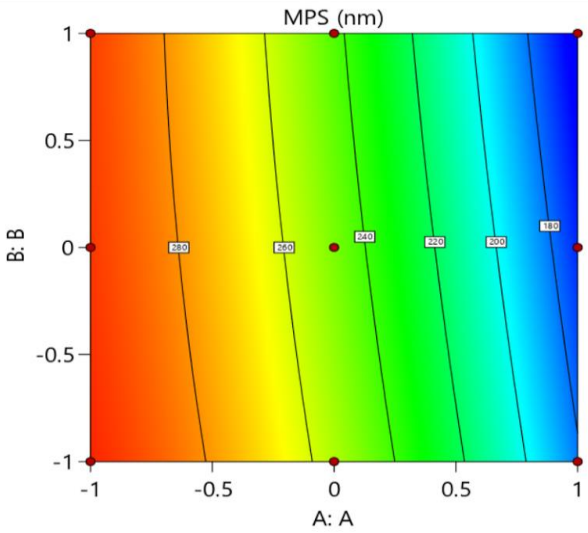

Figure 16. Contour plot

Numerical Optimization

The desirability bar chart Figure 17 shows the desirability values of factors and responses in the optimization solution obtained in the previous step. There were horizontal bars across each factor or response variable with its desirability score ranging from 0 to 1. Two factors, one labeled A and the other B, were represented by blue bars whose ends reached rightwards to the scale's limit, denoting the maximum desirability of one. The responses EE and MPS were depicted by two orange bars. MPS had a desirability of 0.87963 while MPS had the highest desirability of 1. There was also a combined overall desirability bar in orange, and this had a value of 0.87963. The color coding distinguished between the factors in blue from responses in orange color. This visualization showed the extent to which each element met the defined criteria during the optimization process. factor A and B fully complemented the criteria as they had a perfect desirability score. Nevertheless, the EE response and the overall combined desirability showed that it was still possible to fine-tune the optimization further to reach the desired goals.

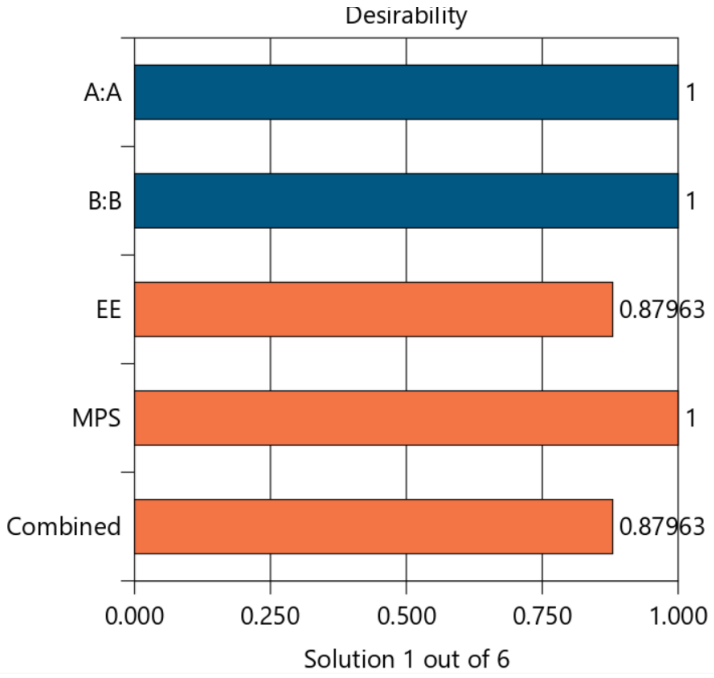

Figure 17. Desirability Bar Chart for Variables A, B, EE, MPS, and Combined Response

Graphical optimization

Specifically, the figure illustrated an interface for adjusting response criteria for a variable referred to as EE. On the left, the options were response variables – EE was chosen, while the other option was MPS. The analysis options at the top revealed that the optimization was oriented to EE. A one-sided interval option was available, but it was not controlled, so a two-sided range was chosen. Specifically, the EE values were brought to a range of 75 to 89, which defines the allowed range of response. The figure below depicts a range of 56 to 89 along the x-axis. A step plot illustrated values within the range of 75 and 89 within the shaded area while the rest, below 75 and above 89, were outside the shaded area. In summary, the interface also offered limit settings to confine the EE response variable between 75 and 89. The step plot represented the areas where EE values would achieve or miss the optimization criteria. Beyond the lower plateau, EE values were defined as unsatisfactory, the range defined by the flat step satisfied the target response criteria in the analysis.

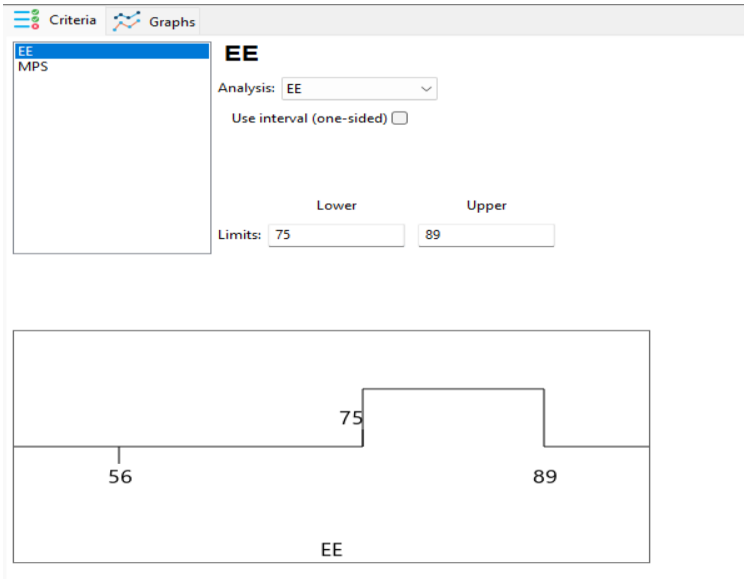

Figure 18. An interface for adjusting response criteria for a variable referred to as EE.

Figure 19, depicts an output of statistical or quality control application that appeared to monitor the Mean Performance Score (MPS). The selected analysis shown above was for MPS at different time points. The previous performance had established a lower limit of 165 and an upper limit of 220, thus providing an acceptable range of performance. Below these limit settings, a basic step plot provides a graphical representation of the interval ranging from the 165 lower limits to the 220 upper limit. This step graph is used to show the defined acceptable range between 165 and 220 with the help of horizontal plot steps to represent the values that fall within the limits specified. The graphical upper boundary stretched to a higher value of 299 probably showing the maximum possible scores of MPS while the acceptable performance was defined only up to 220 as per the analysis limits shown. In general, the chart demonstrated that the chosen metric should be within the range of 165-220, and the threshold values were set to define scores that might indicate the need to control the quality more strictly.

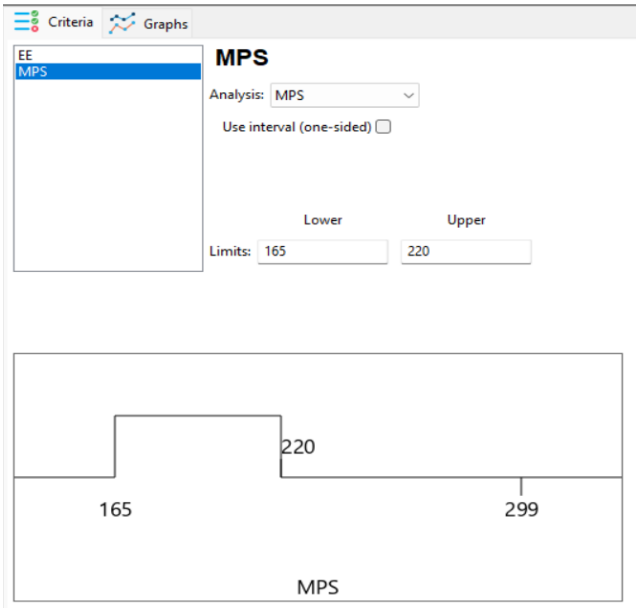

Figure 19. MPS (Mean Particle Size) Analysis with Defined Limits of 165 to 220 nm

Overlay Plot

The overlay plot in Figure 20 illustrated two response surfaces, namely Efficiency (EE) and Mean Performance Score (MPS) against the factors A and B where the x-axis represented a range of A values from about -1.37 to 2.63. The y-axis depicted the range of B values ranging between -1.63 and +2.37. A yellow feasible region in the

middle pointed out the optimal A-B values where EE and MPS were both within the limit. Areas outside this region are those that exhibited A-B values that could not produce acceptable response levels. Annotated values within the plot (e.g. EE: 75, MPS: 165) paired with different A-B points. Specific A-B combinations tested during the past experiment were indicated by red dots. The yellow strip indicated the zone where MPS was between 165 and 220 while EE achieved its objectives. The plot shows which A-B points gave responses in the desired range of values. The use of a factor tool helped in the modification of A and B to identify possible combinations that could be optimal. In summary, the overlay plot from the experimental results was useful in showing results across factors, defining the feasible operating spaces based on multiple responses, and directing future tests to improve the system.

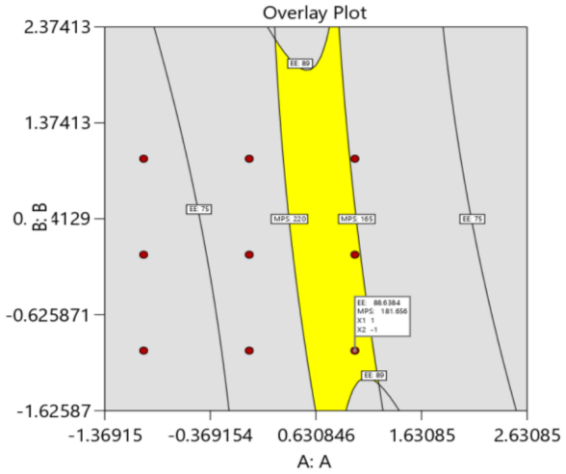

Figure 20. Overlay Plot

The overlay plot Figure 21 presented displayed two response variables, which were Efficiency (EE) on the y-axis and Mean Performance Score (MPS) on the x-axis. The x-axis for Factor A varied from about -2.32 to 5.67 while the y-axis for Factor B ranged from roughly -3.38 to 4.62. Some values of EE, for example, 75 and 89, as well as MPS, such as 165 and 220, were labeled at different points within the feasible region in Figure 21. The desirable or ideal range for both responses was shown in a yellow area in the center of the screen. This was surrounded by gray areas representing areas that were out-of-range responses. Some of the red dot design points obtained from the experiments were in the yellow favorable region while others were in the gray unfavorable region. There was a factor toolbar on the right-hand side which allowed for manipulations of the two factors A and B, and capabilities to go to specific runs, choose terms, and input unique factor values. In general, this overlay plot showed the acceptable ranges of Factor A and Factor B that would lead to acceptable EE and MPS responses, with the yellow area indicating the feasible range that would allow for meeting both requirements.

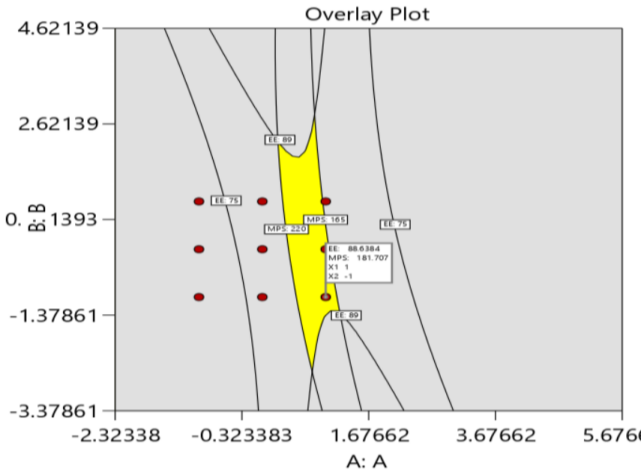

Figure 21. Overlay plot

ZP: Zeta Potential

The particle size analysis done by the Microtrac FLEX Particle Size Analyzer gave information on particle distribution and zeta potential measurement for a sample with identification number Aishwarya M. 25.04.24. The analysis was done on 23rd April 2024 at 7:15 PM with the help of an instrument with serial number W4098 and the software version used was 12.0.0.2. The x-axis displayed the particle sizes in nm of the sample while the y-axis indicated the percentage of the sample that fell under that size range. The curve shows that the size of 126.8 nm was the most frequent particle size within the size range. The zeta potential of the synthesized nanoparticles was found to be -25.3 ± 1.3 mV with a mobility of 3.8 um/V/cm and a conductivity of 330 uS/cm. Field strength was 17.2/18.8 kV/m for 60 seconds. More sample information was given out the 0.727 viscosity and 25.0°C temperature. The particle size percentiles indicated that 50% of the particles were 126.8 nm, 10% were below 106.0 nm and 90% were below 168.0 nm. The zeta potential distribution graph represented the stability characteristics. In the measurement details, this was recorded as 706 and run 1 of 1 with an RMS residual of 0.218%. From the given detailed data, the dispersion and stability characteristics of the tested sample were revealed.

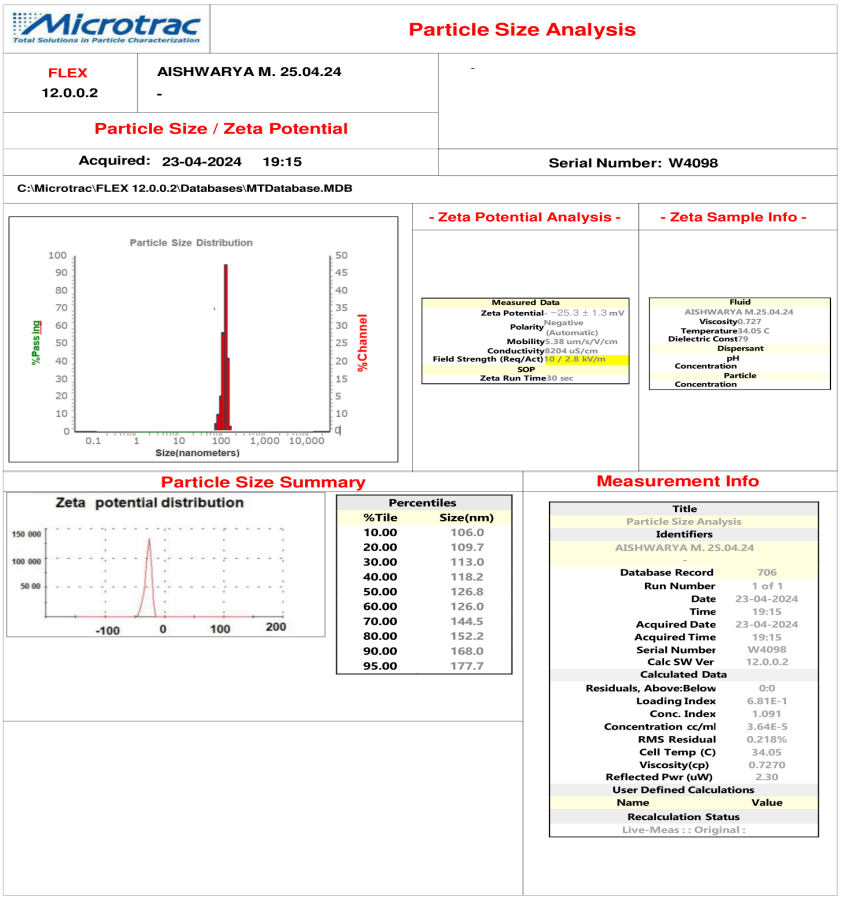

Figure 22. Particle Size Analysis.

DSC: Differential Scanning Calorimetry

The differential scanning calorimetry (DSC) measurement was done on a sample with the label “D H1 H2” that had a mass of 3.000 mg. The reference pan was left empty. A sample was heated from 30 °C to 350 °C at a ramp rate of 10 °C/min and with a gas flow rate of 0.2 mL/min. The DSC curve represented the flow of heat in milliwatts against temperature in degrees Celsius. Two obvious endothermic peaks were detected in the thermogram corresponding to this process. The first endothermic event referred to the following parameters of the process: temperature 157.8°C, onset temperature 157.8°C, peak temperature 157.8°C, and heat flow -160.8mW. This showed that the sample made an endothermic phase change at this temperature, which could be melting or decomposition, and this needed 160.8mW of heat flow. The second endothermic peak was identified at 190.2°C, with the onset and peak temperature at 190.2°C and heat flow of -25.4 mW. This was another distinctly

endothermic transition accompanied by a lesser heat flow of -25.4 mW. DSC analysis showed that the sample experienced two unique endothermic phase transition temperatures of 157.8°C and 190.2°C and a heat flux of 160.8 mW and 25.4 mW respectively in Figure 23. The data acquired can be used to describe characteristics of the heat transfer and phase transition temperatures and energies corresponding to the material.

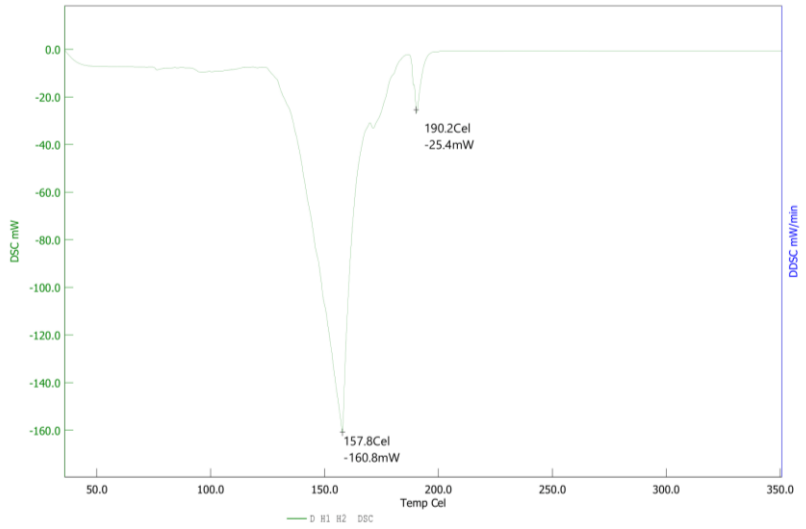

Figure 23. Differential Scanning Calorimetry (DSC) Analysis

SEM: Scanning Electron Microscopy

The scanning electron microscope (SEM) micrograph offered a high-power resolution of the sample's surface relief and topography in Figure. This image was taken at 30,000X using 11.6 mm WD and 20.0 kV HV with Everhart-Thornley detector. The horizontal field width was determined to be 9.95 µm wide. A scale bar of 2.0 µm was added to the images to enable the determination of size. In the micrograph, there are several different particulate features of irregular shapes distributed across the non-uniform background. Three particles with sizes between 84 n and 248 n were highlighted directly on the image according to their size in nanometers. This implied that at the nanoscale level, there were many particle surface structures with different characteristics, hence the seemingly large variation in particle dimensions. This method of SEM inspection and quantification of morphological traits in this manner provided a useful tool in the research context for material sciences, nanotechnology, and other related fields where understanding of nanotopography is critical. The image offered close-up vision into the surface features that could not be observed through normal eye sighting.

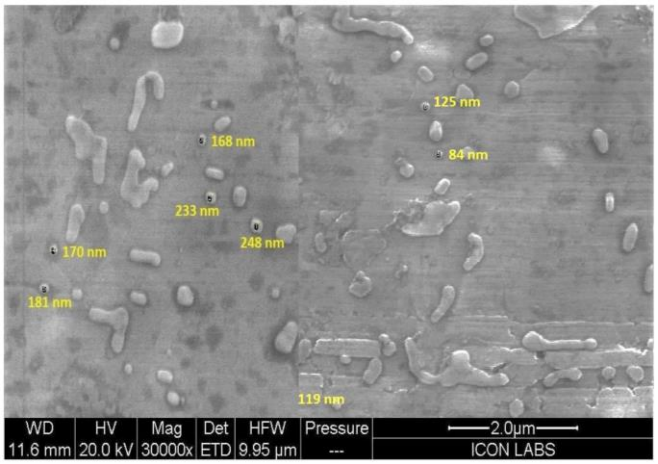

Conclusion

It is important to note that this study achieved the objective of optimizing a solid lipid nanoparticle formulation containing docetaxel using the principles of QbD, which provided a means of understanding and controlling the effect of critical formulation and process variables. The optimized nanoparticles were found to be more stable,

had high entrapment efficiency for the poorly soluble docetaxel, and had a controlled release profile. The supplementation of synergistic herbal extracts adds to the therapeutic value of this nanoformulation. These findings establish the foundation for the optimized docetaxel-loaded lipid nanoparticles to address the challenges of conventional docetaxel therapy such as solubility, toxicity, and chemoresistance. The bioactive herbal extracts also possess complementary anticancer properties when administered with docetaxel making the cocktail therapy. This nanoformulation can be considered a targeted delivery system that can accumulate more in the tumor tissue due to the EPR effect, which makes it a highly promising approach for breast cancer therapy. Additional in vivo studies in other animal models of breast carcinoma can build on the anticancer efficacy and safety profile of this co-delivery strategy before moving to the clinic. In a nutshell, this rational QbD-based design of a combination nano-drug delivery system provides an effective, safe, and patient-centered approach to targeted breast cancer treatment.

References

1. Anayyat, U., Ahad, F., Muluh, T. A., Zaidi, S. A. A., Usmani, F., Yang, H., Li, M., Hassan, H. A., & Wang, X. (2023). Immunotherapy: Constructive Approach for Breast Cancer Treatment. *Breast cancer (Dove Medical Press)*, *15*, 925–951. https://doi.org/10.2147/BCTT.S424624
2. Cardoso, F., Paluch-Shimon, S., Senkus, E., Curigliano, G., Aapro, M. S., André, F., Barrios, C. H., Bergh, J., Bhattacharyya, G. S., Biganzoli, L., Boyle, F., Cardoso, M. J., Carey, L. A., Cortés, J., El Saghir, N. S., Elzayat, M., Eniu, A., Fallowfield, L., Fra
3. ncis, P. A., Gelmon, K., Winer, E. P. (2020). 5th ESO-ESMO international consensus guidelines for advanced breast cancer (ABC 5). *Annals of oncology : official journal of the European Society for Medical Oncology*, *31*(12), 1623–1649. https://doi.org/10.1016/j.annonc.2020.09.010
4. Han, N. R., Park, H. J., Ko, S. G., & Moon, P. D. (2024). Stigmasterol Exerts an Anti-Melanoma Property through Down-Regulation of Reactive Oxygen Species and Programmed Cell Death Ligand 1 in Melanoma Cells. *Antioxidants (Basel, Switzerland)*, *13*(3), 380. https://doi.org/10.3390/antiox13030380
5. Koopaei, M. N., Dinarvand, R., Amini, M., Rabbani, H., Emami, S., Ostad, S. N., & Atyabi, F. (2011). Docetaxel immunonanocarriers as targeted delivery systems for HER 2-positive tumor cells: preparation, characterization, and cytotoxicity studies. *International journal of nanomedicine*, *6*, 1903–1912. https://doi.org/10.2147/IJN.S23211
6. Kumari, A., & Yadav, S. K. (2011). Cellular interactions of therapeutically delivered nanoparticles. *Expert opinion on drug delivery*, *8*(2), 141–151. https://doi.org/10.1517/17425247.2011.547934
7. Müller, R. H., Mäder, K., & Gohla, S. (2000). Solid lipid nanoparticles (SLN) for controlled drug delivery - a review of the state of the art. *European journal of pharmaceutics and biopharmaceutics: official journal of Arbeitsgemeinschaft fur Pharmazeutische Verfahrenstechnik e.V*, *50*(1), 161–177. https://doi.org/10.1016/s0939-6411(00)00087-4
8. Naguib, Y. W., Rodriguez, B. L., Li, X., Hursting, S. D., Williams, R. O., 3rd, & Cui, Z. (2014). Solid lipid nanoparticle formulations of docetaxel prepared with high melting point triglycerides: in vitro and in vivo evaluation. *Molecular pharmaceutics*, *11*(4), 1239–1249. https://doi.org/10.1021/mp4006968
9. Siegel, R. L., Miller, K. D., Fuchs, H. E., & Jemal, A. (2020). Cancer Statistics, 2020. CA: A Cancer Journal for Clinicians, ISSN 0361-3993, 2004, Vol. 70, No. 1, pp. 7–30. https://doi.org/10.3322/caac.21590
10. Soni, G., Kale, K., Shetty, S., Gupta, M., & Yadav, K. S. (2020). Quality by design (QbD) approach in processing polymeric nanoparticles loading anticancer drugs by high pressure homogenizer. *Heliyon*, *6*(4), e03846. https://doi.org/10.1016/j.heliyon.2020.e03846
11. Tang, X., Loc, W. S., Dong, C., Matters, G. L., Butler, P. J., Kester, M., Meyers, C., Jiang, Y., & Adair, J. H. (2017). The use of nanoparticulates to treat breast cancer. *Nanomedicine (London, England)*, *12*(19), 2367–2388. https://doi.org/10.2217/nnm-2017-0202